RF *Performance and Radiation Tolerance Improvement in GaN-based HEMTs using Extremely Thin h-BN Layer and Air Spacer*

S.-J. Chang*, J. Jeong, H.-W. Jung, S.-I. Kim, S.-H. Lee, H.-K. Ahn, D.-M. Kang, J.-W. Lim
RF/Power Component Research Section
Electronics and Telecommunications Research Institute
Daejeon, Korea
*Email: sjchang@etri.re.kr

S. Moon
Department of Materials Science and Engineering
Ajou University
Suwon, Korea

D.-S. Kim
Korea Multi-Purpose Accelerator Complex
Korea Atomic Energy Institute
Gyeongju, Korea

J. Kim, S. I. Im, J. Song
C. Ji, S. Pak, J. K. Kim
Department of Materials Science and Engineering
Pohang University of Science and Technology
Pohang, Korea

***Abstract*— GaN-based high electron mobility transistors (HEMTs) employing thin (≈ 4.36 nm) h-BN passivation layer and an air spacer under the T-gate head were successfully demonstrated for RF performance and radiation tolerance improvement. When their DC characteristics were compared with those of conventional SiN passivated GaN-based HEMTs, the differences were negligible. However, the RF performance, in terms of current gain cut-off frequency and maximum oscillation frequency was significantly improved due to the reduced parasitic capacitances resulting from the low dielectric constant of air. In addition, after γ-ray irradiation, the GaN-based HEMTs with the thin h-BN passivation layer and air spacer exhibited negligible degradation in device properties compared to the conventional SiN passivated GaN-based HEMTs, owing to the absence of the radiation-sensitive SiN passivation layer. Therefore, the immunity to γ-ray irradiation was also efficiently improved.**

Keywords—h-BN, Air Spacer, GaN, HEMT, Passivation, RF Performance, Radiation Tolerance

I. INTRODUCTION

GaN-based high electron mobility transistors (HEMTs) have been intensively studied not only for the high-power microwave applications but also for aerospace applications due to their superior material properties, such as high breakdown field, wide band-gap, high displacement energy, and high carrier density and mobility at the hetero-interface [1-3]. However, numerous dangling bonds which existed at the barrier surface caused leakage current, current collapse, drain current reduction, and frequency performance deterioration [4-6]. Therefore, a passivation layer formed on top of the barrier layer was essentially required. From this perspective, various dielectric materials have been investigated as a passivation layer (and/or system) in GaN-based HEMTs [7-10].

The passivation layer which exhibited excellent layer and interface quality effectively screened the dangling bonds and improved the device performance. However, the passivation layer, in combination with the T-gate electrode, induced parasitic capacitances particularly, the gate-source capacitance (C_{gs}), gate-drain capacitance (C_{gd}), and source-drain capacitance (C_{sd}). Thereby, the radio-frequency (RF) performance in terms of current-gain cut-off frequency (f_T) and maximum oscillation frequency (f_{max}) was limited by the device passivation [11]. In addition, compared with GaN, the passivation layer showed weaker radiation tolerance [12,13]. The overall radiation tolerance of GaN-based HEMTs was largely determined by the passivation layer. Therefore, the device passivation has a significant impact on both RF performance and radiation tolerance.

In this study, we introduced a novel passivation structure to simultaneously improve RF performance and radiation tolerance in GaN-based HEMTs. A 4.36 nm-thick h-BN passivation layer and an air spacer located under the T-gate head were implemented for the fabrication of GaN-based HEMTs. The conventional SiN passivation layer was replaced with an extremely thin h-BN passivation layer and an air spacer. When compared with the SiN passivated GaN-based HEMTs (i.e., Sample B), the DC characteristics of the GaN-based HEMTs employing the thin h-BN passivation layer and air spacer (i.e., Sample A) were nearly identical. However, Sample A showed lower parasitic capacitances than Sample B, since the dielectric constant of the air was smaller than that of SiN. As a result, the f_T and f_{max} in Sample A were improved by 50% and 68%, respectively, compared with those of in Sample B. Moreover, although the parasitic capacitances of Sample B increased by γ-ray irradiation, the increase in parasitic capacitances was negligible in Sample A due to the absence of the dielectrics layer, demonstrating superior radiation hardness.

II. DEVICE FABRICATION

The AlGaN/GaN heterostructure was grown by metal organic chemical vapor deposition (MOCVD) on a 2-inch SiC substrate. It consisted of a 2 µm-thick Fe-doped GaN buffer, 100 nm-thick GaN channel, and 25 nm-thick $Al_{0.25}Ga_{0.75}N$ barrier. A thin h-BN passivation layer was then grown on the AlGaN barrier using MOCVD, as described elsewhere [14,15]. A 50 nm-thick SiN protection layer was deposited on top of the thin passivation layer. The source and drain ohmic contact areas were defined using an i-line stepper. The SiN protection layer and h-BN passivation layer were etched using a reactive ion etching (RIE) system. Ohmic metal stacks (i.e., Ti/Al/Ni/Au) were deposited by an e-beam evaporator. The SiN protection layer was removed using a buffered oxide etchant (BOE) to

This research was supported by the National Research Council of Science & Technology (NST) grant by the Korea government (MIST) (No. GTL25051-000).

prevent the diffusion of alloying metal into the SiN protection layer during the rapid thermal annealing (RTA) process. RTA was then carried out at 880°C for 30 s to form the source and drain ohmic contact. Subsequently, a 50 nm-thick SiN protection layer was redeposited. Device isolation was achieved by phosphorus implantation outside the device active area. Since the SiN protection layer was damaged during the isolation process, it was removed using BOE. A final 75 nm-thick SiN protection layer was then deposited. The source and drain contact pads were defined and etched using the i-line stepper and RIE, respectively. To from the contact pads, Ti/Au was deposited by the e-beam evaporator. The gate foot (i.e., gate length) was patterned using an e-beam lithography. To etch the 75 nm-thick SiN and thin h-BN layers, an inductively coupled plasma etching process was employed. Afterwards, the e-beam lithography process was again performed to define the T-gate head pattern, followed by Ni/Au deposition using the e-beam evaporator for the formation of the gate electrode. Finally, the fabricated wafer was dipped into BOE to remove the final 75 nm-thick SiN protection layer. The MOCVD grown h-BN passivation layer was chemically stable and did not dissolve in BOE, enabling a high selectivity over SiN during BOE etching. As a result, only the thin h-BN passivation layer was remained, and an air spacer was formed between the h-BN passivation layer and T-gate head.

The gate length (L_G), unit gate width (W_G), number of fingers (N_F), source-to-gate distance (L_{SG}), and gate-to-drain distance (L_{GD}) of the fabricated devices were 0.15 µm, 100 µm, 2, 1.0 µm, and 1.85 µm, respectively. For comparison of device performance and radiation tolerance, conventional SiN passivated GaN-based HEMTs were simultaneously processed.

In Fig. 1, we have conducted a detailed microstructural investigation of the fabricated GaN-based HEMTs (Sample A) to confirm the formation of the air spacer and existence of thin h-BN passivation layer. The cross-section of the T-gate region and the thin h-BN passivation layer were examined using a focused ion beam (FIB) and transmission electron microscope, respectively. The air spacer formed between the T-gate head and the thin h-BN passivation layer was observed by cross-sectional imaging. The thickness of the thin h-BN passivation layer was measured to be approximately 4.36 nm.

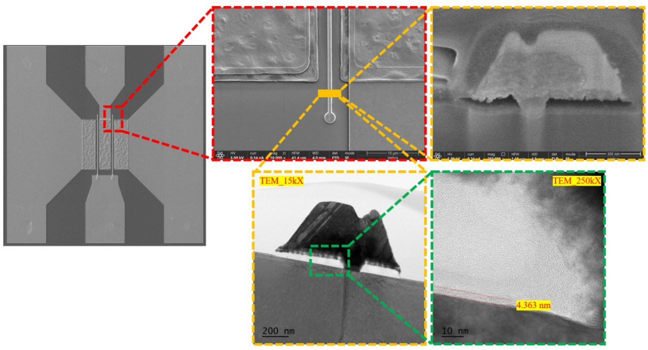

Fig. 1. Microscopic measurements in GaN-based HEMTs with thin h-BN passivation layer and air spacer. The cross-section of the T-gate region and h-BN passivation layer was investigated by FIB and TEM, respectively.

III. Results and Discussion

A. DC Characteristics

For comparison of the DC properties corresponding to the device passivation, we measured the typical transfer characteristics in Sample A and Sample B, as shown in Fig. 2. Both samples exhibited superior pinch-off characteristics at low gate bias ($V_{GS} < -4.5$ V). In the subthreshold regime, the drain current (I_D) curves overlapped. The threshold voltages (V_{TH}) which were determined by plotting $\sqrt{I_D}$ versus V_{GS} and extrapolated the line to zero I_D [16] were extracted as -3.38 V and -3.29 V for Sample A and Sample B, respectively. The leakage current (I_{Dleak}) was lower at $V_{GS} < -4.5$ V in Sample A compared with Sample B attributed to the excellent h-BN/AlGaN interface quality based on Van der Waals bonding [15]. The saturation I_D reached to 750 mA/mm at V_{GS} = -0.5 V. Well behaved bell-shaped transconductance (g_m) was achieved for the two samples. Except for I_{Dleak}, the difference in transfer characteristics including V_{TH}, saturation I_D, and maximum g_m was negligible for the two samples.

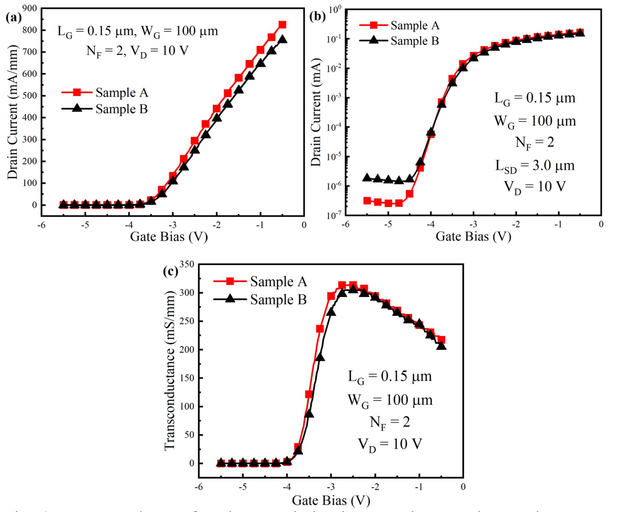

Fig. 2. Measured transfer characteristics in Sample A and Sample B. I_D *vs.* V_{GS} in (a) linear scale and (b) logarithmic scale. (c) g_m as a function of V_{GS}.

In Fig. 3, we compared the output characteristics which were associated with the output power of the GaN-based HEMTs. In Sample B, I_D was saturated at $V_{DS} \approx 2.5$ V due to the self-heating effects [17,18]. However, in Sample A, I_D continued to increase slightly but consistently at $V_{DS} > 2.5$ V due to the diminished self-heating effects by the formation of the air spacer.

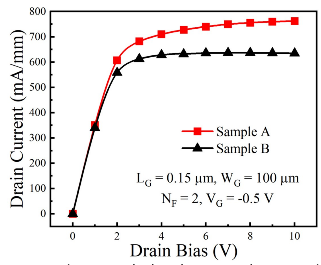

Fig. 3. Measured output characteristics in Sample A and Sample B. I_D as a function of V_D.

B. RF Performance

In Fig. 4, the RF performance in terms of f_T and f_{max} was measured with respect to the device passivation, since these parameters were representative indicators to reflect the RF performance. For the extraction of f_T and f_{max}, S-parameters were measured using a network analyzer. We converted the measured S-parameters to H-parameters. A linear line with a -20 dB/decade slope was fitted to the H_{21} curve. We defined the f_T as the extrapolated frequency of the linear line reached 0 dB. To extract f_{max}, we converted the measured S-parameter to the maximum stable gain / maximum, available gain. We fitted a linear line with -20 dB/decade slope at the stability factor K = 1. The extrapolated frequency of the linear line reached 0 dB was defined as the f_{max}. Compared with Sample B, we have obtained a huge RF performance improvement in Sample A. The f_T and f_{max} were increased by 50% and 68%, respectively.

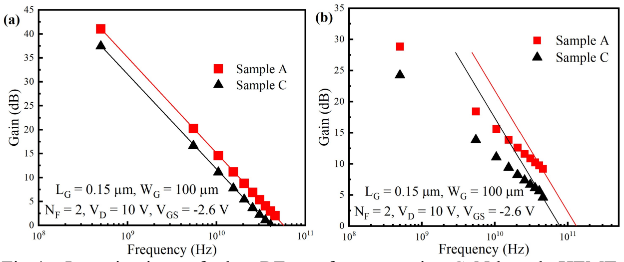

Fig.4. Investigation of the RF performance in GaN-based HEMTs corresponding to the device passivation. Gain *vs*. frequency for (a) f_T and (b) f_{max}.

To figure out the RF performance improvement in Sample A, we have extracted the parasitic capacitances such as C_{gs}, C_{gd}, and C_{sd}, since they were affected by the gate structure and device passivation. The three parasitic capacitances were extracted using the method described in [11]. The S-parameters were measured under cold-FET conditions and converted into Y-parameters for capacitance extraction. Since all devices share identical layout, the differences reflect variations in intrinsic capacitances caused by the different passivation layer. The extracted parasitic capacitances were lower in Sample A than in Sample B. In Sample A, the SiN passivation layer used in Sample B was mostly replaced with the air spacer. The dielectric constant of air was smaller than that of SiN. Thereby, the parasitic capacitances were reduced in Sample A, achieving RF performance improvement in Sample A.

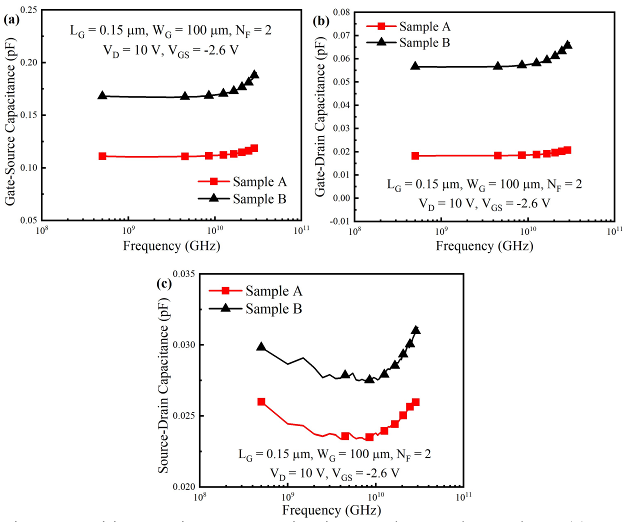

Fig.5. Parasitic capacitance extraction in Sample A and Sample B. (a) C_{gs}, (b) C_{gd}, and (c) C_{sd} as a function of frequency.

C. Radiation Tolerance

To compared the radiation tolerance with respect to the device passivation, γ-ray irradiation was performed on Sample A and Sample B. The γ-ray irradiation was carried out at the Advanced Radiation Technology Institute. The radiated γ-ray dose was 1.5 Mrad(Si) with the dose rate of 50 rad/s. The electrical measurements were conducted for the two samples before and after γ-ray irradiation, and the dependence of the DC and RF characteristics on γ-ray irradiation was compared.

We measured the transfer characteristics after γ-ray irradiation and compared them with those obtained before γ-ray irradiation, as shown in Fig. 6. The change in the DC characteristics such as V_{TH}, $g_{m,max}$, and I_{Dleak} was much smaller in Sample A than in Sample B. This phenomenon was because γ-ray irradiation mostly induced total ionizing dose effects in dielectric materials (i.e., the SiN passivation layer) rather than displacement damages in semiconductor materials [19] in Sample B. In Sample B, the SiN passivation layer contained K^O defect centers with neutral charges. The K^O defect centers were converted into K^+ defect centers with positive charge by γ-ray irradiation. Thereby, the device properties were altered by γ-ray irradiation in Sample B [20]. In contrast, no dielectric material susceptible to γ-ray irradiation was present in Sample A. Therefore, Sample A exhibited much lower sensitivity to γ-ray irradiation than Sample B, exhibiting smaller device property change generated by γ-ray irradiation in Sample A.

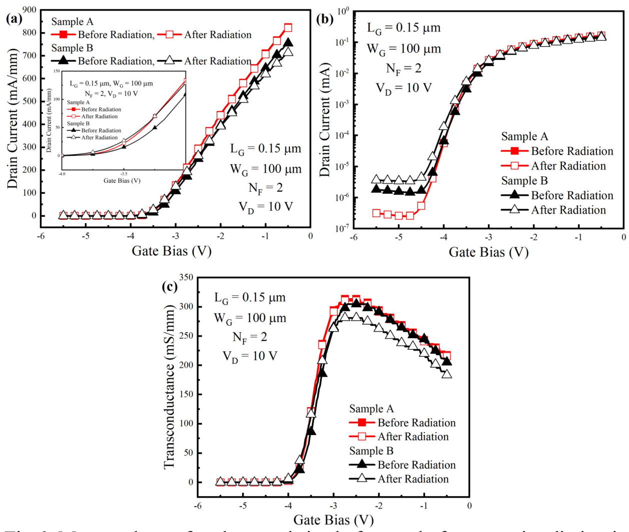

Fig.6. Measured transfer characteristics before and after γ-ray irradiation in Sample A and Sample B. I_D *vs*. V_{GS} in (a) linear scale and (b) logarithmic scale. (c) g_m as a function of V_{GS}. Inset showed in Fig. 6(a) the zoomed-in I_D *vs*. V_{GS} curves at $V_{GS} \approx V_{TH}$.

The RF performance in terms of f_T and f_{max} was also extracted and compared before and after γ-ray irradiation according to the device passivation. Similar to the DC characteristics, the RF performance degradation in Sample B was much larger compared with the Sample A. In Sample B, f_T and f_{max} were deteriorated by 20% and 18%, respectively. In contrast, the RF performance degradation in Sample A was negligible.

To understand why the radiation tolerance was stronger in Sample A than in Sample B, we extracted parasitic capacitances before and after γ-ray irradiation. In Sample B, the parasitic capacitances such as C_{gs}, C_{gd}, and C_{sd} were increased by γ-ray irradiation. However, the parasitic capacitances in Sample A were not affected by γ-ray irradiation. These results indicated that γ-ray irradiation deteriorated the quality of SiN passivation layer [12,19,20]. Therefore, the parasitic capacitances which were related to the passivation system increased by γ-ray irradiation in Sample B. In Sample A, the SiN passivation layer was mostly replaced with the air spacer, and no dielectric material sensitive to γ-ray irradiation was present. Therefore, the parasitic capacitances in Sample A were barely independent to γ-ray irradiation, demonstrating strong immunity to γ-ray irradiation.

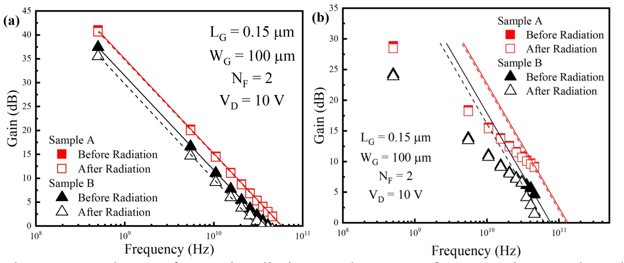

Fig.7. Dependence of γ-ray irradiation on the RF performance in GaN-based HEMTs corresponding to the device passivation. Extracted (a) f_T and (b) f_{max} in Sample A and Sample B before and after γ-ray irradiation.

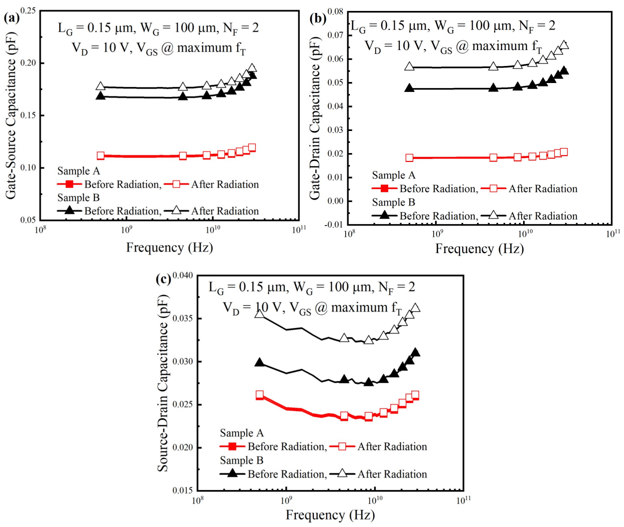

Fig.8. Parasitic capacitances compared before and after γ-ray irradiation in Sample A and Sample B. (a) C_{gs}, (b) C_{gd}, and (c) C_{sd} as a function of frequency.

IV. Conclusion

This work has confirmed the feasibility of employing extremely thin h-BN as a device passivation layer in GaN-based HEMTs. We demonstrated GaN-based HEMTs applying the extremely thin h-BN passivation layer grown by MOCVD and air spacer under the T-gate head. Identical DC characteristics were achieved when compared with conventional SiN passivated GaN-based HEMTs. However, the RF performance in terms of f_T and f_{max} was improved by 50% and 68%, respectively, due to the reduction of parasitic capacitances resulting from the low dielectric constant of air. In addition, GaN-based HEMTs with the thin h-BN passivation layer and air spacer exhibited superior radiation tolerance. The SiN passivation layer which was deteriorated by the γ-ray irradiation was substituted by the air spacer. No dielectric material which was vulnerable to γ-ray irradiation was present, improving radiation tolerance. As a result, we simultaneously achieved the RF performance improvement and strong radiation tolerance through the employment of the thin h-BN passivation layer and air spacer in GaN-based HEMTs.

References

[1] T. Yang, K. Shinohara, D. Regan, et al., "Ultrahigh-speed GaN high-electron-mobility transistors with f_T/f_{max} of 454/444 GHz," *IEEE Electron Device Lett.*, vol. 36, pp. 549-551, 2015.

[2] T. Palacios, A. Chakraborty, S. Rajan, et al., "High-power AlGaN/GaN HEMTs for Ka-band Applications," *IEEE Electron Device Lett.*, vol. 26, pp. 781-783, 2005.

[3] K. Shinohara, D. C. Regan, Y. Tang, et al., "Scaling of GaN HEMTs and Schottky diodes for submillimeter-wave MMIC applications," *IEEE Trans. Electron Dev.*, vol. 60, pp. 2982-2996, 2013.

[4] R. Vetury, N. Q. Zhang, S. Keller, and U. K. Mishra, "The impact of surface states om the DC and RF characteristics of AlGaN/GaN HFETs," *IEEE Trans. Electron Dev.*, vol. 48, pp. 560-566, 2001.

[5] B. Green, J. Chu, E. Chumbes, et al., "The effect of surface passivation on the microwave characteristics of undoped AlGaN/GaN HEMTs," *IEEE Electron Device Lett.*, vol. 21, pp. 268-270, 2000.

[6] T. Hashizume, J. Kotani, and H. Hasegawa, "Leakage mechanism in GaN and AlGaN Schottky interface," *Appl. Phys. Lett.*, vol. 84, pp. 4884-4886, 2004.

[7] P. D. Ye, B. Yang, K. Ng, and J. Bude, "GaN metal-oxide-semiconductor high-electron-mobility-transistor with atomic layer deposited Al_2O_3 as gate dielectric," *Appl. Phys. Lett.*, vol. 86, 063501, 2005.

[8] S. Arulkumaran, T. Egawa, H. Ishikawa, et al,, "Surface passivation effects on AlGaN/GaN high-electron-mobility transistors with SiO_2, Si_3N_4, and Silicon oxynitride," *Appl. Phys. Lett.*, vol. 84, pp. 613-615, 2004.

[9] W. Lu, V. Kumar, R. Shwindt, et al., "A comparative study of surface passivation on AlGaN/GaN HEMTs," *Solid-State Electron.*, vol. 46, pp. 1441-1444, 2002.

[10] A. V. Vertiatchikh, L. F. Eastman, W. J. Schaff, and T. Prunty, "Effect of surface passivation of AlGaN/GaN heterostructure field-effect transistor," *Electronics Lett.*, vol. 38, pp. 388-389, 2002.

[11] A. Jarndal and G. Kompa, "A new small-signal modeling approach applied to GaN devices," *IEEE Trans. Microw. Theory Tech.*, vol. 53, pp. 3440-3448, 2005.

[12] S.-J. Chang, D.-S. Kim, T.-W. Kim, et al., "Comprehensive research of total ionizing dose effects in GaN-based MIS-HEMTs using extremely thin gate dielectric layer," *nanomaterials*, vol. 10(11), 2175, 2020.

[13] Z. Gao, M. F. Romero, A. Redondo-Cubero, et al., "Effects of Gd_2O_3 gate dielectric on proton-irradiated AlGaN/GaN HEMTs," *IEEE Electron Device Lett.*, vol. 38, pp. 611-614, 2017.

[14] S. Moon, S.-J. Chang, Y. Kim, et al., "Van der Waals heterostructure of hexagonal boron nitride with and AlGaN/GaN epitaxial wafer for high-performance radio frequency applications," *ACS Appl. Mater. Interfaces*, vol. 13, pp. 59440-59449, 2021.

[15] S. Moon, O. F. N. Okello, A. Rousseau, et al., "Wafer-scale AA-stacked hexagonal boron nitride grown on a GaN substrate," *Nature Materials*, pp. 1-9, 2015.

[16] H. G. Lee, S. Y. Oh, and G. Fuller, "A simple and accurate method to measure the threshold voltage of an enhancement-mode MOSFET," *IEEE Trans. Electron Dev.*, vol. 29(2), pp. 346-348, 1982.

[17] S. Karmalkar and U. K. Mishra, "Enhancement of breakdown voltage in AlGaN/GaN high electron mobility transistors using a filed place," *IEEE Trans. Electron Dev.*, vol. 148, pp. 1515-1521, 2001.

[18] S.-J. Chang, K.-J. Cho, S.-Y. Lee, et al., "Substrate effects on the electrical properties in GaN-based high electron mobility transistors," *Crystals*, vol. 11, 1414, 2021.

[19] S. Kaya, I. Yildiz, R. Lik. E. Yilmax, "Co-60 gamma radiation effects on DC, RF, and pulsed I-V characteristics of AlGaN/GaN HEMTs," *Solid-State Electron.*, vol. 48, pp. 471-475, 2018.

[20] P. Dong, X. Yu, Y. Ma, et al., "A deep-level transit spectroscopy study of gamma-ray irradiation on the passivaiton properties of silicon nitride layer on silicon," AIP adv., vol. 7(8), 085112, 2017.